

# Boosting Generative Image Modeling via Joint Image-Feature Synthesis

**Theodoros Kouzelis**  
Archimedes, Athena RC  
National Technical University of Athens

**Efstathios Karypidis**  
Archimedes, Athena RC  
National Technical University of Athens

**Ioannis Kakogeorgiou**  
Archimedes, Athena RC  
IIT, NCSR "Demokritos"

**Spyros Gidaris**  
valeo.ai

**Nikos Komodakis**  
Archimedes, Athena RC  
University of Crete  
IACM-Forth

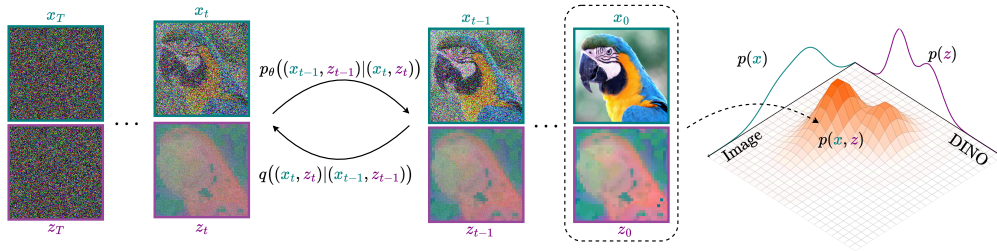


Figure 1: ReDi: Our generative image modeling framework bridges the gap between generative modeling and representation learning by leveraging a diffusion model that jointly captures low-level image details (via VAE latents) and high-level semantic features (via DINOv2). Trained to generate coherent image–feature pairs from pure noise, this unified latent-semantic dual-space diffusion approach significantly boosts both generative quality and training convergence speed.

## Abstract

Latent diffusion models (LDMs) dominate high-quality image generation, yet integrating representation learning with generative modeling remains a challenge. We introduce a novel generative image modeling framework that seamlessly bridges this gap by leveraging a diffusion model to jointly model low-level image latents (from a variational autoencoder) and high-level semantic features (from a pretrained self-supervised encoder like DINO). Our latent-semantic diffusion approach learns to generate coherent image–feature pairs from pure noise, significantly enhancing both generative quality and training efficiency, all while requiring only minimal modifications to standard Diffusion Transformer architectures. By eliminating the need for complex distillation objectives, our unified design simplifies training and unlocks a powerful new inference strategy: Representation Guidance, which leverages learned semantics to steer and refine image generation. Evaluated in both conditional and unconditional settings, our method delivers substantial improvements in image quality and training convergence speed, establishing a new direction for representation-aware generative modeling. Project page and code: <https://representationdiffusion.github.io/>

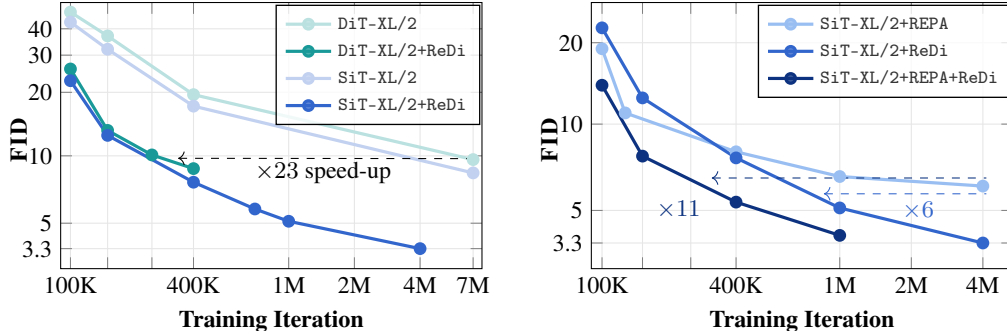


Figure 2: **Accelerated Training.** Generative performance curves on Imagenet  $256 \times 256$  without Classifier-Free Guidance. **Left:** Our ReDi accelerates convergence of DiT-XL/2 and SiT-XL/2 by approximately  $\times 23$  speed-up. **Right:** ReDi converges  $\times 6$  faster than REPA. When applied on top of REPA delivers a  $\times 11$  speed-up.

## 1 Introduction

Latent diffusion models (LDMs) (Rombach et al., 2022) have emerged as a leading approach for high-quality image synthesis, achieving state-of-the-art results (Rombach et al., 2022; Peebles & Xie, 2023; Ma et al., 2024). These models operate in two stages: first, a variational autoencoder (VAE) compresses images into a compact latent representation (Rombach et al., 2022); second, a diffusion model learns the distribution of these latents, capturing their underlying structure.

Leveraging their intermediate features, pretrained LDMs have shown promise for various scene understanding tasks, including classification (Mukhopadhyay et al., 2023), pose estimation (Gong et al., 2023), and segmentation (Li et al., 2023b; Liu et al., 2023; Delatolas et al., 2025). However, their discriminative capabilities typically underperform specialized (self-supervised) representation learning approaches like masking-based (He et al., 2022), contrastive (Chen et al., 2020), self-distillation (Caron et al., 2021), or vision-language contrastive (Radford et al., 2021a) methods. This limitation stems from the inherent tension in LDM training - the need to maintain precise low-level reconstruction while simultaneously developing semantically meaningful representations.

This observation raises a fundamental question: *How can we leverage representation learning to enhance generative modeling?* Recent work by Yu et al. (2025) (REPA) demonstrates that improving the semantic quality of diffusion features through distillation of pretrained self-supervised representations leads to better generation quality and faster convergence. Their results establish a clear connection between representation learning and generative performance.

Motivated by these insights, we investigate whether a more effective approach to leveraging representation learning can further enhance image generation performance. In this work, we contend that the answer is *yes*: rather than aligning diffusion features with external representations via distillation, we propose to *jointly model both images (specifically their VAE latents) and their high-level semantic features* extracted from a pretrained vision encoder (e.g., DINOv2 (Oquab et al., 2024)) within the same diffusion process. Formally, as shown in Figure 1, we define the forward diffusion process as  $q(\mathbf{x}_t, \mathbf{z}_t | \mathbf{x}_{t-1}, \mathbf{z}_{t-1})$  for  $t = 1, \dots, T$ , where  $\mathbf{x}_0 = \mathbf{x}$  and  $\mathbf{z}_0 = \mathbf{z}$  are the clean VAE latents and semantic features, respectively. The reverse process  $p_\theta(\mathbf{x}_{t-1}, \mathbf{z}_{t-1} | \mathbf{x}_t, \mathbf{z}_t)$  learns to gradually denoise both modalities from Gaussian noise.

This joint modeling approach forces the diffusion model to explicitly learn the joint distribution of both precise low-level (VAE) and high-level semantic (DINOv2) features. We implement this approach, called ReDi (Representation Diffusion), within the DiT (Peebles & Xie, 2023) and SiT (Ma et al., 2024) frameworks with minimal modifications to their transformer architecture: we apply standard diffusion noise to both representations, combine them into a single set of tokens, and train the standard diffusion transformer architecture to denoise both components simultaneously.

Compared to REPA, our joint modeling approach offers three key advantages. First, the diffusion process explicitly models both low-level and semantic features, enabling direct integration of these complementary representations. Second, our method simplifies training by eliminating the need for additional distillation objectives. Finally, during inference, our unified approach enables *Representation Guidance* - where the model uses its learned semantic understanding to iteratively refine generated images, improving quality in both conditional and unconditional generation.

Our contributions can be summarized as follows:

1. We propose **ReDi**, a novel and effective method that jointly models image-compressed latents and semantically rich representations within the diffusion process, significantly improving image synthesis performance.
2. We provide a concrete implementation of our approach for both diffusion (DiT) and flow-matching (SiT) frameworks, leveraging DINOv2 (Oquab et al., 2024) as the source of high-quality semantic representations.
3. We also introduce *Representation Guidance*, which leverages the model’s semantic predictions during inference to refine outputs, further enhancing image generation quality.
4. We demonstrate that our approach boosts performance in both conditional and unconditional generation, while significantly accelerating convergence (see Figure 2).

## 2 Related work

**Representation Learning.** Various approaches aim to learn meaningful representations for downstream tasks, with self-supervised learning emerging as one of the most promising directions. Early approaches employed pretext tasks such as predicting image patch permutations (Noroozi & Favaro, 2016) or rotation angles (Gidaris et al., 2018), while more recent methods utilize contrastive learning (Chen et al., 2020; Van den Oord et al., 2018; Misra & Maaten, 2020), clustering-based objectives (Caron et al., 2020, 2018, 2019), and self-distillation techniques (Grill et al., 2020; Chen & He, 2021; Caron et al., 2021; Gidaris et al., 2021). The introduction of transformers enabled Masked Image Modeling (MIM), introduced by BEiT (Bao et al., 2022) and evolved through SimMIM (Xie et al., 2022), MAE He et al. (2022), AttMask (Kakogeorgiou et al., 2022), iBOT (Zhou et al., 2022), and MOCA (Gidaris et al., 2024), with DINOv2 (Oquab et al., 2024) achieving state-of-the-art performance through scaled models and datasets. Separately, contrastive vision-language pretraining, initiated by CLIP (Radford et al., 2021a), established powerful joint image-text representations. Subsequent models like SigLIP Zhai et al. (2023) and SigLIPv2 (Tschannen et al., 2025) refined this framework through enhanced training techniques, excelling in zero-shot settings and image retrieval (Kordopatis-Zilos et al., 2025). Building on these advances, we leverage pretrained DINOv2 visual representations to enhance image generative modeling performance.

**Diffusion Models and Representation Learning** Due to the success of diffusion models, many recent works leverage representations learned from pre-trained diffusion models for downstream tasks (Fuest et al., 2024). In particular, intermediate U-Net (Ronneberger et al., 2015) features have been shown to capture rich semantic information, enabling tasks such as semantic segmentation (Baranchuk et al., 2022; Zhao et al., 2023), semantic correspondence (Luo et al., 2023; Zhang et al., 2023; Hedlin et al., 2023), depth estimation (Zhao et al., 2023), and image editing (Tumanyan et al., 2023). Furthermore, diffusion models have been used for knowledge transfer by distilling learned representations through teacher-student frameworks (Li et al., 2023a) or refining them via reinforcement learning (Yang & Wang, 2023). Other works have shown that diffusion models learn strong discriminative features that can be leveraged for classification (Mukhopadhyay et al., 2023; Xiang et al., 2023). In a complementary direction, REPA (Yu et al., 2025) recently demonstrated that aligning the internal representations of DiT (Peebles & Xie, 2023) with a powerful pre-trained visual encoder during training significantly improves generative performance. Motivated by this observation, we propose to integrate images and semantic representations into a joint learning process.

**Multi-modal Generative Modeling** Unifying the generation across diverse modalities has recently attracted widespread interest. Notably, CoDi (Tang et al., 2023) leverages a diffusion model that enables generation across text, image, video, and audio in an aligned latent space. A joint representation for different modalities has been shown to have great scalability properties (Mizrahi et al., 2023). For video generation, WVD (Zhang et al., 2024) incorporates explicit 3D supervision by

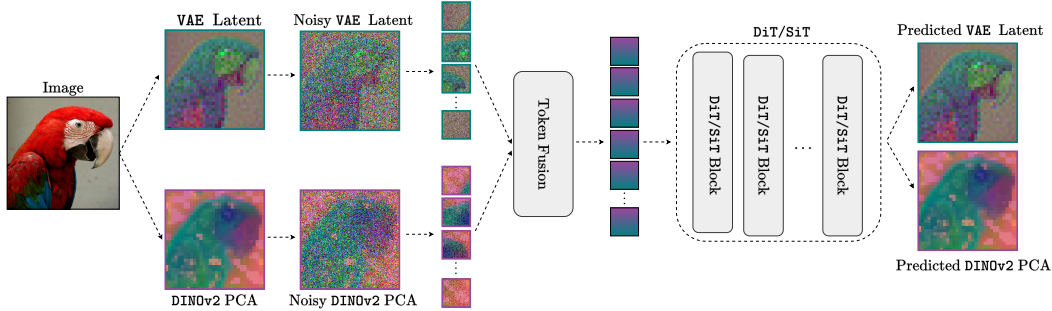


Figure 3: Given an input image, the VAE latent and the principal components of DINOv2 are extracted. Both modalities are noised and fused into a *joint token sequence*, given as input to DiT or SiT.

learning the joint distribution of RGB and XYZ frames. To capture richer spatial semantics, GEM (Hassan et al., 2024) generates paired images and depth maps. MT-Diffusion (Chen et al., 2024) learns to incorporate various multi-modal data types with a multitask loss including CLIP (Radford et al., 2021b) image representations. However, they do not quantitatively assess how this impacts the generative performance. VideoJam (Chefer et al., 2025) models a joint image-motion representation that boosts temporal coherence and introduces a theoretically motivated Classifier-Free Guidance (CFG) Ho & Salimans (2022) variant to condition on both motion and text. Inspired by this approach and building on the standard CFG framework, we propose Representation Guidance, incorporating the visual representations as an additional guidance signal during inference.

### 3 Method

#### 3.1 Preliminaries

**Denosing Diffusion Probabilistic Models (DDPM)** Diffusion models (Ho et al., 2020) generate data by gradually denoising a noisy input. The forward process corrupts an input  $\mathbf{x}_0$  (e.g., an image or its VAE latent) over  $T$  steps by adding Gaussian noise:

$$\mathbf{x}_t = \sqrt{\bar{\alpha}_t} \mathbf{x}_0 + \sqrt{1 - \bar{\alpha}_t} \epsilon, \quad (1)$$

where  $\mathbf{x}_t$  is the noisy input at step  $t$ ,  $\bar{\alpha}_t$  are constants that define the noise schedule, and  $\epsilon \sim \mathcal{N}(\mathbf{0}, \mathbf{I})$  is the Gaussian noise term. Following Ho et al. (2020), the reverse process learns to denoise  $\mathbf{x}_t$  by predicting the added noise  $\epsilon$  using a network  $\epsilon_\theta(\cdot)$  with parameters  $\theta$ . The training objective is:

$$\mathcal{L}_{simple} = \mathbb{E}_{\mathbf{x}_0, \epsilon, t} \|\epsilon_\theta(\mathbf{x}_t, t) - \epsilon\|^2. \quad (2)$$

Although we also include the variational lower bound loss from Nichol & Dhariwal (2021) to learn the variance of the reverse process, we omit it hereafter for brevity.

Unless otherwise specified, we focus on class-conditional image generation throughout this work. For notational simplicity, we omit explicit class conditioning variables from all mathematical formulations.

**Diffusion Transformers (DiT)** The DiT Peebles & Xie (2023) implements  $\epsilon_\theta$  using a Vision Transformer Dosovitskiy et al. (2021). Given the “patchified” input  $\mathbf{x}_t \in \mathbb{R}^{L \times C_x}$  ( $L$  tokens of dimension  $C_x$ ), the model first computes embeddings:

$$\mathbf{h}_t = \mathbf{x}_t \mathbf{W}_{emb}, \quad \mathbf{W}_{emb} \in \mathbb{R}^{C_x \times C_d}. \quad (3)$$

The transformer processes  $\mathbf{h}_t \in \mathbb{R}^{L \times C_d}$  to produce  $\mathbf{o}_t \in \mathbb{R}^{L \times C_d}$ . The final noise prediction is computed as:

$$\epsilon_\theta(\mathbf{x}_t, t) = \mathbf{o}_t \mathbf{W}_{dec}, \quad \mathbf{W}_{dec} \in \mathbb{R}^{C_d \times C_x}. \quad (4)$$

#### 3.2 Joint Image-Representation Generation

Our goal is to train a single model to jointly generate images and their semantic-aware visual representations by modeling their shared probability distribution. This approach captures the interdependent

structures and features of both modalities. While we frame our approach using DDPM, it is also applicable to models trained with flow-matching objectives Ma et al. (2024) (see Appendix A).

A high-level overview of our method is depicted in Figure 3. Let  $I$  denote a clean image,  $\mathbf{x}_0 = \mathcal{E}_x(I) \in \mathbb{R}^{L \times C_x}$  its VAE tokens (produced by the VAE encoder  $\mathcal{E}_x(\cdot)$ ), and  $\mathbf{z}_0 = \mathcal{E}_z(I) \in \mathbb{R}^{L \times C_z}$  its patch-wise visual representation tokens (extracted by a pretrained encoder  $\mathcal{E}_z(\cdot)$ , e.g., DINOv2 Oquab et al. (2024))<sup>1</sup>. To match the spatial resolution of  $\mathbf{x}_0$ , we assume  $\mathcal{E}_z(\cdot)$  includes a bilinear resizing operation.

During training, given  $\mathbf{x}_0$  and  $\mathbf{z}_0$ , we define a joint forward diffusion processes:

$$\mathbf{x}_t = \sqrt{\bar{\alpha}_t} \mathbf{x}_0 + \sqrt{1 - \bar{\alpha}_t} \epsilon_x, \quad \mathbf{z}_t = \sqrt{\bar{\alpha}_t} \mathbf{z}_0 + \sqrt{1 - \bar{\alpha}_t} \epsilon_z, \quad (5)$$

where  $\bar{\alpha}_t$  controls the noise schedule and  $\epsilon_x \sim \mathcal{N}(\mathbf{0}, \mathbf{I})$ ,  $\epsilon_z \sim \mathcal{N}(\mathbf{0}, \mathbf{I})$  are Gaussian noise terms of dimensions  $\mathbb{R}^{L \times C_x}$  and  $\mathbb{R}^{L \times C_z}$ , respectively.

The diffusion model  $\epsilon_\theta(\mathbf{x}_t, \mathbf{z}_t, t)$  takes as input  $\mathbf{x}_t$  and  $\mathbf{z}_t$ , along with timestep  $t$ , and jointly predicts the noise for both inputs. Specifically, it produces two separate predictions:  $\epsilon_\theta^x(\mathbf{x}_t, \mathbf{z}_t, t)$  for the image latent noise  $\epsilon_x$ , and  $\epsilon_\theta^z(\mathbf{x}_t, \mathbf{z}_t, t)$  for the visual representation noise  $\epsilon_z$ . The training objective combines both predictions:

$$\mathcal{L}_{joint} = \mathbb{E}_{\mathbf{x}_0, \mathbf{z}_0, t} \left[ \|\epsilon_\theta^x(\mathbf{x}_t, \mathbf{z}_t, t) - \epsilon_x\|^2 + \lambda_z \|\epsilon_\theta^z(\mathbf{x}_t, \mathbf{z}_t, t) - \epsilon_z\|^2 \right], \quad (6)$$

where  $\lambda_z$  balances the denoising loss for  $\mathbf{z}_t$ . By default, we use  $\lambda_z = 1$  in our experiments.

### 3.3 Fusion of Image and Representation Tokens

We explore two approaches to combine and jointly process  $\mathbf{x}_t$  and  $\mathbf{z}_t$  in the diffusion transformer architecture: (1) merging tokens along the embedding dimension, and (2) maintaining separate tokens for each modality (see Fig. 4). Both methods require only minimal modifications to the DiT architecture, specifically defining modality-specific embedding matrices  $\mathbf{W}_{emb}^x \in \mathbb{R}^{C_x \times C_d}$  and  $\mathbf{W}_{emb}^z \in \mathbb{R}^{C_z \times C_d}$ , along with prediction heads  $\mathbf{W}_{dec}^x \in \mathbb{R}^{C_d \times C_x}$  and  $\mathbf{W}_{dec}^z \in \mathbb{R}^{C_d \times C_z}$  for  $\mathbf{x}_t$  and  $\mathbf{z}_t$  respectively.

**Merged Tokens** The tokens are embedded separately and summed channel-wise:

$$\mathbf{h}_t = \mathbf{x}_t \mathbf{W}_{emb}^x + \mathbf{z}_t \mathbf{W}_{emb}^z \in \mathbb{R}^{L \times C_d}. \quad (7)$$

The transformer processes  $\mathbf{h}_t$  to produce  $\mathbf{o}_t$ , with predictions:

$$\epsilon_\theta^x = \mathbf{o}_t \mathbf{W}_{dec}^x, \quad \epsilon_\theta^z = \mathbf{o}_t \mathbf{W}_{dec}^z. \quad (8)$$

This approach enables early fusion while maintaining computational efficiency, as the token count remains unchanged.

**Separate Tokens** Tokens are embedded separately and concatenated along the sequence dimension:

$$\mathbf{h}_t = [\mathbf{x}_t \mathbf{W}_{emb}^x, \mathbf{z}_t \mathbf{W}_{emb}^z] \in \mathbb{R}^{2L \times C_d}, \quad (9)$$

where  $[\cdot, \cdot]$  denotes sequence-wise concatenation. The transformer outputs separate representations  $\mathbf{o}_t = [\mathbf{o}_t^x, \mathbf{o}_t^z]$ , with predictions:

$$\epsilon_\theta^x = \mathbf{o}_t^x \mathbf{W}_{dec}^x, \quad \epsilon_\theta^z = \mathbf{o}_t^z \mathbf{W}_{dec}^z. \quad (10)$$

This method provides greater expressive power by preserving modality-specific information throughout processing, at the cost of increased computation due to increased token count.

Unless stated otherwise, we use the merged tokens approach for computational efficiency.

<sup>1</sup>For notational clarity, we incorporate the patchification step (typically with  $2 \times 2$  patches in DiT architectures) into the encoder definitions  $\mathcal{E}_x$  and  $\mathcal{E}_z$ .

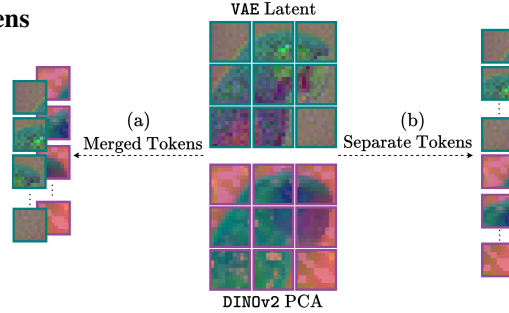


Figure 4: An illustration of our proposed token fusion approaches: (a) The tokens of the VAE latents and the DINOv2 are merged channel-wise, (b) The tokens are concatenated along the sequence dimension.

### 3.4 Dimensionality-Reduced Visual Representation

In practice, the channel dimension of visual representations ( $C_z$ ) significantly exceeds that of image latents ( $C_x$ ), i.e.,  $C_z \gg C_x$ . We empirically observe that this imbalance degrades performance, as the model disproportionately allocates capacity to visual representations at the expense of image latents.

To address this, we apply Principal Component Analysis (PCA) to reduce the dimensionality of  $\mathbf{z}_0$  from  $C_z$  to  $C'_z$  (where  $C'_z \ll C_z$ ), preserving essential information while simplifying the prediction task. The PCA projection matrix is precomputed using visual representations sampled from the training set. All visual representations in Sections 3.2 and 3.3 refer to these PCA-reduced versions.

### 3.5 Representation Guidance

To ensure the generated images remain strongly influenced by the visual representations during inference, we introduce Representation Guidance. This technique during inference modifies the posterior distribution to:  $\hat{p}_\theta(\mathbf{x}_t, \mathbf{z}_t) \propto p_\theta(\mathbf{x}_t)p(\mathbf{z}_t|\mathbf{x}_t)^{w_r}$ , where  $w_r$  controls how strongly samples are pushed toward higher likelihoods of the conditional distribution  $p_\theta(\mathbf{z}_t|\mathbf{x}_t)$ . Taking the log derivative yields the guided score function:

$$\nabla_{\mathbf{x}_t} \log \hat{p}_\theta(\mathbf{x}_t, \mathbf{z}_t) = \nabla_{\mathbf{x}_t} \log p_\theta(\mathbf{x}_t) + w_r (\nabla_{\mathbf{x}_t} \log p_\theta(\mathbf{z}_t|\mathbf{x}_t)) \quad (11)$$

$$= \nabla_{\mathbf{x}_t} \log p_\theta(\mathbf{x}_t) + w_r (\nabla_{\mathbf{x}_t} \log p_\theta(\mathbf{x}_t, \mathbf{z}_t) - \nabla_{\mathbf{x}_t} \log p_\theta(\mathbf{x}_t)). \quad (12)$$

By recalling the equivalence of denoisers and scores (Vincent, 2011), we implement this representation-guided prediction  $\hat{e}_\theta(\mathbf{x}_t, \mathbf{z}_t, t)$  at each denoising step as follows:

$$\hat{e}_\theta(\mathbf{x}_t, \mathbf{z}_t, t) = \epsilon_\theta(\mathbf{x}_t, t) + w_r (\epsilon_\theta(\mathbf{x}_t, \mathbf{z}_t, t) - \epsilon_\theta(\mathbf{x}_t, t)). \quad (13)$$

Following Ho & Salimans (2022), we train both  $e_\theta(\mathbf{x}_t, \mathbf{z}_t, t)$  and  $e_\theta(\mathbf{x}_t, t)$  jointly. Specifically, during training, with probability  $p_{drop}$ , we zero out  $\mathbf{z}_t$  (setting  $\epsilon_\theta(\mathbf{x}_t, t) = \epsilon_\theta(\mathbf{x}_t, \mathbf{0}, t)$ ) and disable the visual representation denoising loss by setting  $\lambda_z = 0$  in Equation 6.

## 4 Experiments

### 4.1 Setup

**Implementation details.** We follow the standard training setup of DiT (Peebles & Xie, 2023) and SiT (Ma et al., 2024), training on ImageNet at  $256 \times 256$  resolution with a batch size of 256. Following ADM’s preprocessing pipeline (Dhariwal & Nichol, 2021), we center-crop and resize all images to  $256 \times 256$ . Our experiments utilize transformer architectures B/2, L/2, and XL/2 all using a  $2 \times 2$  patch size. For unconditional generation, we simply set the number of classes to 1, maintaining the original architecture. Images are encoded into VAE latent representations using SD-VAE-FT-EMA (Rombach et al., 2022) that produces outputs with  $\times 8$  spatial downsampling factor and 4 output channels. For  $256 \times 256$  images, this results in  $32 \times 32 \times 4$  latent features. Through patchification with  $2 \times 2$  patches, the VAE encoder  $\mathcal{E}_x(\cdot)$  yields  $L = 256$  tokens, each with  $C_x = 16$  channels (4 channels  $\times 2 \times 2$  patch size). For semantic representation extraction, we employ DINOv2-B with registers (Darcet et al., 2023; Oquab et al., 2024). The 768-dimensional embeddings are reduced to 8 dimensions via PCA (trained on 76,800 randomly sampled ImageNet images). After bilinear interpolation to match the VAE’s  $32 \times 32 \times 4$  spatial resolution and  $2 \times 2$  patchification, the encoder  $\mathcal{E}_z(\cdot)$  produces  $L = 256$  tokens with  $C_z = 32$  channels each (8 channels  $\times 2 \times 2$  patch size).

**Sampling.** For DiT models, we adopt DDPM sampling, while for SiT models, we employ the SDE Euler–Maruyama sampler. The number of sampling steps is fixed at 250 across all experiments. When using Classifier-Free Guidance (CFG) (Ho & Salimans, 2022), we apply it only to the VAE channels, with a guidance scale of  $w = 2.4$  (see Figure 6). For Representation Guidance, we set  $p_{drop} = 0.2$ , the guidance scale to  $w_r = 1.5$  for B models and  $w_r = 1.1$  for XL models.

**Evaluation.** To benchmark generative performance, we report Frechet Inception Distance (FID) (Heusel et al., 2017), sFID (Nash et al., 2021), Inception Score (IS) (Salimans et al., 2016), Precision (Pre.) and Recall (Rec.) (Kynkäänniemi et al., 2019) using 50k samples and the ADM’s TensorFlow evaluation suite (Dhariwal & Nichol, 2021).

Table 1: **FID Comparisons.** FID scores on ImageNet  $256 \times 256$  without Classifier-Free Guidance for DiT and SiT models of various sizes with REPA and ReDi (ours).

MODEL	#PARAMS	ITER.	FID↓
DiT-L/2	458M	400K	23.2
w/ REPA	458M	400K	15.6
w/ ReDi (ours)	458M	400K	10.5
SiT-L/2	458M	400K	18.5
w/ REPA	458M	400K	9.7
w/ ReDi (ours)	458M	400K	9.4
DiT-XL/2	675M	400K	19.5
w/ REPA	675M	400K	12.3
DiT-XL/2	675M	7M	9.6
w/ REPA	675M	850K	9.6
w/ ReDi (ours)	675M	400K	8.7
SiT-XL/2	675M	400K	17.2
w/ REPA	675M	400K	7.9
w/ ReDi (ours)	675M	400K	7.5
SiT-XL/2	675M	7M	8.3
w/ REPA	675M	4M	5.9
w/ ReDi (ours)	675M	700K	5.6
w/ ReDi (ours)	675M	4M	3.3

Table 2: **Comparison with State-of-the-art.** Quantitative evaluation on ImageNet  $256 \times 256$  with Classifier-Free Guidance. Both REPA and ReDi (ours) employ SiT-XL/2 as the base model.

MODEL	EPOCHS	FID↓	SFID↓	IS↑	PRE.↑	REC.↑
<i>Autoregressive Models</i>						
VAR	350	1.80	-	365.4	0.83	0.57
MagViTv2	1080	1.78	-	319.4	0.83	0.57
MAR	800	1.55	-	303.7	0.81	0.62
<i>Latent Diffusion Models</i>						
LDM	200	3.60	-	247.7	0.87	0.48
U-ViT-H/2	240	2.29	5.68	263.9	0.82	0.57
DiT-XL/2	1400	2.27	4.60	278.2	0.83	0.57
MaskDiT	1600	2.28	5.67	276.6	0.80	0.61
SD-DiT	480	3.23	-	-	-	-
SiT-XL/2	1400	2.06	4.50	270.3	0.82	0.59
FasterDiT	400	2.03	4.63	264.0	0.81	0.60
MDT	1300	1.79	4.57	283.0	0.81	0.61
<i>Leveraging Visual Representations</i>						
REPA	800	1.80	4.50	284.0	0.81	0.61
ReDi (ours)	350	1.72	4.68	278.7	0.77	0.63
ReDi (ours)	800	1.61	4.66	295.1	0.78	0.64

## 4.2 Enhancing the performance of generative models

**DiT & SiT.** To demonstrate the effectiveness of our approach, we present performance gains for various-sized DiT and SiT models in Table 1. Our method, ReDi, consistently delivers substantial improvements across models of different scales. Notably, DiT-XL/2 with ReDi achieves an FID of 8.7 after just 400k iterations, outperforming the baseline DiT-XL/2 trained for 7M steps. Similarly, SiT-XL/2 with ReDi reaches an FID of 7.5 at 400k iterations, surpassing the converged SiT-XL at 7M steps. Additionally, Table 2 reports results for SiT-XL/2 with Classifier-Free Guidance (CFG) Ho & Salimans (2022). Once again, ReDi yields significant improvements, achieving an FID of 1.72 in just 350 epochs, outperforming the baseline trained to convergence over 1400 epochs.

**Comparison with REPA.** We further compare our results with REPA, which also leverages DINOv2 features to enhance generative performance. Our approach, ReDi, consistently achieves superior generative performance with both DiT and SiT as the base models. As shown in Table 1, DiT-L/2 with ReDi achieves an FID of 10.5 significantly outperforming DiT-L/2 with REPA. Notably, it even surpasses REPA trained for the same number of iterations with the larger DiT-XL/2, which achieves a higher FID of 12.3. Further for SiT-XL models, ReDi attains an FID of 5.6 in just 700k iterations, while REPA requires 4M iterations to reach an FID of 5.9. These results highlight the effectiveness of our method in leveraging visual representations to significantly boost generative performance.

**ReDi is complementary to REPA.** Interestingly, we observe that the joint modeling objective of our ReDi and the alignment objective of REPA are complementary. As presented in Table 5 REPA + ReDi matches the FID of the fully-converged REPA after only 350K iterations, and at 1M iterations reaches an FID of 3.6. For the implementation details, see Appendix B.3.

**Accelerating convergence.** The aforementioned results indicate that ReDi significantly accelerates the convergence of latent diffusion models. As illustrated in Figure 2, ReDi speeds up the convergence of DiT-XL/2 and SiT-XL/2 by approximately  $\times 23$ , respectively. Even when compared with REPA, ReDi demonstrated a  $\times 6$  faster convergence. When ReDi is applied on top of REPA, the convergence is  $\times 11$  faster.

**Comparison with state-of-the-art generative models.** Ultimately, we provide a quantitative comparison between ReDi and other recent generative models using Classifier-Free Guidance (CFG)

Table 3: **Unconditional Generation FID Performance.** Results on ImageNet  $256 \times 256$ . For comparison, we include conditional generation results (shown in gray). Models at 400K steps. RG denotes using Representation Guidance.

MODEL	#PARAMS	FID↓
DiT-B/2 (conditional)	130M	43.5
DiT-B/2	130M	69.3
w/ ReDi (ours)	130M	51.7
w/ ReDi+RG (ours)	130M	47.3
DiT-XL/2 (conditional)	675M	19.5
DiT-XL/2	675M	44.6
w/ ReDi (ours)	675M	25.1
w/ ReDi+RG (ours)	675M	22.6

Table 4: **FID with Representation Guidance.** FID scores on ImageNet  $256 \times 256$ . RG denotes Representation Guidance. Models at 400K steps.

MODEL	#PARAMS	FID↓
DiT-B/2 w/ ReDi	130M	25.7
DiT-B/2 w/ ReDi+ RG	130M	20.2
DiT-XL/2 w/ ReDi	675M	8.7
DiT-XL/2 w/ ReDi+ RG	675M	5.9

Table 5: **ReDi with REPA.** FID scores on ImageNet  $256 \times 256$  w/o CFG.

MODEL	#ITER.	FID↓
SiT-XL/2 w/ REPA	4M	5.9
SiT-XL/2 w/ REPA+ReDi	350K	5.9
SiT-XL/2 w/ REPA+ReDi	1M	3.5

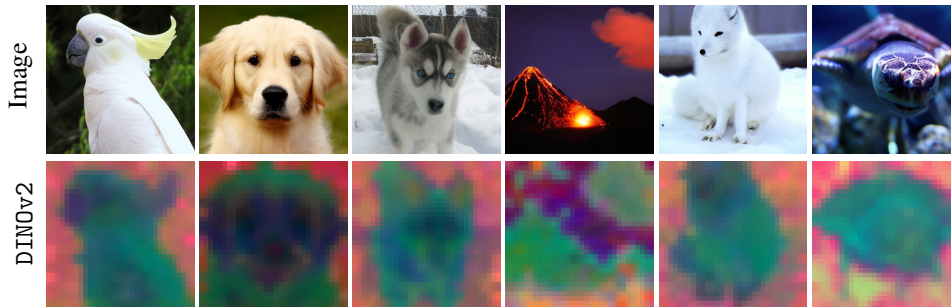


Figure 5: **Selected samples** from our SiT-XL/2 w/ ReDi model trained on ImageNet  $256 \times 256$ . Images and visual representations are jointly generated by our model. We use Classifier-Free Guidance with  $w = 4.0$ .

(Ho & Salimans, 2022) in Table 2. Our method already outperforms both the vanilla SiT-XL and SiT-XL with REPA with only 350 epochs. At 800 epochs ReDi reaches an FID of 1.64. We provide qualitative results of both generated images and visual representations in Figure 5.

**Improving Unconditional Generation.** To establish the effectiveness of our method in improving generative models, we further present experiments for unconditional generation using DiT. As shown in Table 3, our ReDi significantly improves generative performance for various model sizes. Specifically, with our ReDi FID drops from 69.3 to 51.7 for B and from 44.6 to 25.1 for XL models.

### 4.3 Impact of Representation Guidance on generative performance.

**Class Conditional Generation.** In Table 4 we present the impact of Representation Guidance (RG) on generative performance. We observe that for both B and XL models, Representation Guidance unlocks further performance enhancements by guiding the generated image to closely follow the semantic features of DINOv2. Particularly for DiT-XL w/ ReDi the FID drops from 8.7 to 5.9. We also present qualitative results in Figure 8.

**Unconditional Generation.** Representation Guidance is especially useful in unconditional generation scenarios, where the absence of class or text conditioning prevents the use of Classifier-Free Guidance to enhance performance. As demonstrated in Table 3, Representation Guidance enhances the performance of ReDi with both B and XL models, *further closing the performance gap between unconditional and conditional generation*. Notably, ReDi with Representation Guidance achieves an FID of 22.6, approaching the performance of the class-conditioned DiT-XL/2 (FID of 19.5).

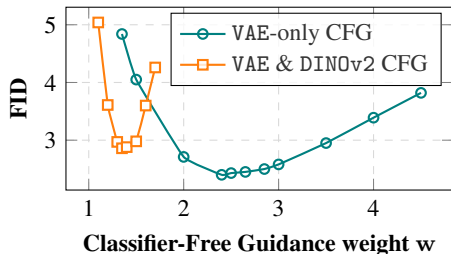


Figure 6: **VAE-only vs. VAE & DINOv2 CFG.** FID scores for SiT-XL with ReDi (trained for 400K steps) as a function of Classifier-Free Guidance weight  $w$ , comparing two configurations: (1) applying CFG only to VAE latents (VAE-only CFG) versus (2) applying CFG to both VAE and DINOv2 representations (VAE & DINOv2 CFG).

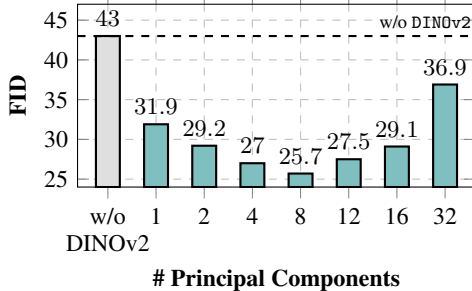


Figure 7: **Effect of number of principal components.** FID of DiT-B/2 w/ ReDi with different number of DINOv2 Principal Components. The vanilla DiT-B/2 is illustrated with gray. No Classifier-Free Guidance is used.

Table 6: **Performance of Modality Combination Strategies.** FID scores on ImageNet  $256 \times 256$  without CFG for DiT-B/2 with ReDi using Separate Tokens (SP) and Merged Tokens (MR). See Appendix B for details on throughput measurements.

MODEL	#TOKENS	THROUGHPUT $\uparrow$	FID $\downarrow$
DiT-B/2	256	4.52	43.5
w/ ReDi (MR)	256	4.51	25.7
w/ ReDi (SP)	512	2.26	24.7

#### 4.4 Analysis

**Dimensionality reduction ablation.** We begin the analysis of our method by ablating the impact of dimensionality reduction on the visual representations, as shown in Figure 7. Initially, we observe that jointly learning as little as one principal component yields significant improvements in generative performance. Increasing the component count continues to improve performance, up to  $r = 8$ , beyond which further components begin to degrade the quality of generation. This suggests an optimal intermediate subspace where compressed visual features retain sufficient expressivity to guide generation without dominating model capacity.

**Merged Tokens vs. Separate Tokens.** In Table 6, we evaluate the effectiveness of the two explored integration strategies, Merged Tokens (MR) and Separate Tokens (SP), for joint learning of image VAE latents and visual representations, using DiT-B/2 as our base model. While both approaches achieve comparable performance gains, SP demonstrates slightly better results. This advantage comes at a significant computational cost: SP doubles the transformer’s input sequence length by introducing 256 additional DINOv2 tokens, resulting in approximately  $2\times$  greater compute demands during both training and inference (Kaplan et al., 2020). The MR strategy, by contrast, maintains the original sequence length while delivering similar performance improvements, thereby preserving computational efficiency as measured by throughput.

**VAE-only Classifier-Free Guidance.** As ReDi jointly models both VAE latents and visual representations, we investigate two Classifier-Free Guidance (CFG) strategies: applying CFG exclusively to VAE latents (VAE-only CFG) versus applying it to both modalities simultaneously (VAE & DINOv2 CFG). Our experiments in Figure 6 demonstrate that VAE-only CFG achieves superior results, yielding an FID of 2.39 compared to 2.86 for the VAE & DINOv2 CFG approach. Notably, VAE-only CFG also shows greater robustness to variations in the CFG weight parameter.

## 5 Conclusion

In this work, we explore the relationship between semantic representation learning and generative performance in latent diffusion models. Building on recent insights, we introduced ReDi, a novel framework that integrates high-level semantic features with low-level latent representations within the diffusion process. Unlike prior approaches that rely on auxiliary objectives, ReDi jointly models the two distributions. We demonstrate that this simple approach is more effective at leveraging the semantic features and leads to drastic improvements in generative performance. We further proposed Representation Guidance, a novel guidance method that leverages the jointly learned semantic features to enhance image quality. Across both conditional and unconditional settings, ReDi consistently improves generation quality and accelerates convergence, highlighting the benefits of our approach.

**Acknowledgements** This work has been partially supported by project MIS 5154714 of the National Recovery and Resilience Plan Greece 2.0 funded by the European Union under the NextGenerationEU Program and by Institute of Informatics and Telecommunications, National Center for Scientific Research “Demokritos”. Hardware resources were granted with the support of GRNET. Also, this work was performed using HPC resources from GENCI-IDRIS (Grants 2024-AD011012884R3).

## References

- Bao, F., Nie, S., Xue, K., Cao, Y., Li, C., Su, H., and Zhu, J. All are worth words: A vit backbone for diffusion models. In *Proceedings of the IEEE/CVF conference on computer vision and pattern recognition*, pp. 22669–22679, 2023.
- Bao, H., Dong, L., Piao, S., and Wei, F. BEit: BERT pre-training of image transformers. In *International Conference on Learning Representations*, 2022.
- Baranchuk, D., Voynov, A., Rubachev, I., Khrukov, V., and Babenko, A. Label-efficient semantic segmentation with diffusion models. In *International Conference on Learning Representations*, 2022. URL <https://openreview.net/forum?id=SlxSY2UZQT>.
- Caron, M., Bojanowski, P., Joulin, A., and Douze, M. Deep clustering for unsupervised learning of visual features. In *Proceedings of the European Conference on Computer Vision*, pp. 132–149, 2018.
- Caron, M., Bojanowski, P., Mairal, J., and Joulin, A. Unsupervised pre-training of image features on non-curated data. In *Proceedings of the IEEE/CVF International Conference on Computer Vision*, pp. 2959–2968, 2019.
- Caron, M., Misra, I., Mairal, J., Goyal, P., Bojanowski, P., and Joulin, A. Unsupervised learning of visual features by contrasting cluster assignments. *Advances in Neural Information Processing Systems*, 33:9912–9924, 2020.
- Caron, M., Touvron, H., Misra, I., Jegou, H., Mairal, J., Bojanowski, P., and Joulin, A. Emerging properties in self-supervised vision transformers. In *ICCV*, 2021.
- Chefer, H., Singer, U., Zohar, A., Kirstain, Y., Polyak, A., Taigman, Y., Wolf, L., and Sheynin, S. Videojam: Joint appearance-motion representations for enhanced motion generation in video models. *arXiv preprint arXiv:2502.02492*, 2025.
- Chen, C., Ding, H., Sisman, B., Xu, Y., Xie, O., Yao, B. Z., Tran, S. D., and Zeng, B. Diffusion models for multi-modal generative modeling. *arXiv preprint arXiv:2407.17571*, 2024.
- Chen, T., Kornblith, S., Norouzi, M., and Hinton, G. A simple framework for contrastive learning of visual representations. In *ICML*, 2020.
- Chen, X. and He, K. Exploring simple siamese representation learning. In *Proceedings of the IEEE/CVF Conference on Computer Vision and Pattern Recognition*, pp. 15750–15758, 2021.
- Darcet, T., Oquab, M., Mairal, J., and Bojanowski, P. Vision transformers need registers. *arXiv preprint arXiv:2309.16588*, 2023.

- Delatolas, T., Kalogeiton, V., and Papadopoulos, D. P. Studying image diffusion features for zero-shot video object segmentation. *arXiv preprint arXiv:2504.05468*, 2025.
- Dhariwal, P. and Nichol, A. Q. Diffusion models beat GANs on image synthesis. In *NeurIPS*, 2021.
- Dosovitskiy, A., Beyer, L., Kolesnikov, A., Weissenborn, D., Zhai, X., Unterthiner, T., Dehghani, M., Minderer, M., Heigold, G., Gelly, S., et al. An image is worth 16x16 words: Transformers for image recognition at scale. In *ICLR*, 2021.
- Elfwing, S., Uchibe, E., and Doya, K. Sigmoid-weighted linear units for neural network function approximation in reinforcement learning. *Neural networks*, 107:3–11, 2018.
- Fuest, M., Ma, P., Gui, M., Schusterbauer, J., Hu, V. T., and Ommer, B. Diffusion models and representation learning: A survey. *arXiv preprint arXiv:2407.00783*, 2024.
- Gao, S., Zhou, P., Cheng, M.-M., and Yan, S. Mdtv2: Masked diffusion transformer is a strong image synthesizer. *arXiv preprint arXiv:2303.14389*, 2023.
- Gidaris, S., Singh, P., and Komodakis, N. Unsupervised representation learning by predicting image rotations. In *International Conference on Learning Representations*, 2018.
- Gidaris, S., Bursuc, A., Puy, G., Komodakis, N., Cord, M., and Pérez, P. Obow: Online bag-of-visual-words generation for self-supervised learning. In *CVPR*, 2021.
- Gidaris, S., Bursuc, A., Siméoni, O., Vobecký, A., Komodakis, N., Cord, M., and Perez, P. MOCA: Self-supervised representation learning by predicting masked online codebook assignments. *Transactions on Machine Learning Research*, 2024.
- Gong, J., Foo, L. G., Fan, Z., Ke, Q., Rahmani, H., and Liu, J. Diffpose: Toward more reliable 3d pose estimation. In *Proceedings of the IEEE/CVF Conference on Computer Vision and Pattern Recognition (CVPR)*, June 2023.
- Grill, J.-B., Strub, F., Altché, F., Tallec, C., Richemond, P., Buchatskaya, E., Doersch, C., Avila Pires, B., Guo, Z., Gheshlaghi Azar, M., et al. Bootstrap your own latent—a new approach to self-supervised learning. *Advances in Neural Information Processing Systems*, 33:21271–21284, 2020.
- Hassan, M., Stapf, S., Rahimi, A., Rezende, P., Haghighi, Y., Brüggemann, D., Katircioglu, I., Zhang, L., Chen, X., Saha, S., et al. Gem: A generalizable ego-vision multimodal world model for fine-grained ego-motion, object dynamics, and scene composition control. *arXiv preprint arXiv:2412.11198*, 2024.
- He, K., Chen, X., Xie, S., Li, Y., Dollár, P., and Girshick, R. Masked autoencoders are scalable vision learners. In *CVPR*, 2022.
- Hedlin, E., Sharma, G., Mahajan, S., Isack, H., Kar, A., Tagliasacchi, A., and Yi, K. M. Unsupervised semantic correspondence using stable diffusion. In *Thirty-seventh Conference on Neural Information Processing Systems*, 2023. URL <https://openreview.net/forum?id=sovXUzPzLN>.
- Heusel, M., Ramsauer, H., Unterthiner, T., Nessler, B., and Hochreiter, S. Gans trained by a two time-scale update rule converge to a local nash equilibrium. *Advances in neural information processing systems*, 30, 2017.
- Ho, J. and Salimans, T. Classifier-free diffusion guidance. *arXiv preprint arXiv:2207.12598*, 2022.
- Ho, J., Jain, A., and Abbeel, P. Denoising diffusion probabilistic models. *Advances in neural information processing systems*, 33:6840–6851, 2020.
- Kakogeorgiou, I., Gidaris, S., Psomas, B., Avrithis, Y., Bursuc, A., Karantzaos, K., and Komodakis, N. What to hide from your students: Attention-guided masked image modeling. In *ECCV*, 2022.
- Kaplan, J., McCandlish, S., Henighan, T., Brown, T. B., Chess, B., Child, R., Gray, S., Radford, A., Wu, J., and Amodei, D. Scaling laws for neural language models. *arXiv preprint arXiv:2001.08361*, 2020.

- Kordopatis-Zilos, G., Stojnić, V., Manko, A., Šuma, P., Ypsilantis, N.-A., Efthymiadis, N., Laskar, Z., Matas, J., Chum, O., and Toliás, G. ILIAS: Instance-level image retrieval at scale, 2025.
- Kynkäänniemi, T., Karras, T., Laine, S., Lehtinen, J., and Aila, T. Improved precision and recall metric for assessing generative models. *Advances in neural information processing systems*, 32, 2019.
- Li, D., Ling, H., Kar, A., Acuna, D., Kim, S. W., Kreis, K., Torralba, A., and Fidler, S. Dreamteacher: Pretraining image backbones with deep generative models. In *Proceedings of the IEEE/CVF International Conference on Computer Vision*, pp. 16698–16708, 2023a.
- Li, T., Tian, Y., Li, H., Deng, M., and He, K. Autoregressive image generation without vector quantization. *arXiv preprint arXiv:2406.11838*, 2024.
- Li, Z., Zhou, Q., Zhang, X., Zhang, Y., Wang, Y., and Xie, W. Open-vocabulary object segmentation with diffusion models. 2023b.
- Lipman, Y., Chen, R. T. Q., Ben-Hamu, H., Nickel, M., and Le, M. Flow matching for generative modeling. In *The Eleventh International Conference on Learning Representations*, 2023. URL <https://openreview.net/forum?id=PqvMRDCJT9t>.
- Liu, J., Hu, T., Sonke, J.-j., and Gavves, E. Beyond generation: Exploring generalization of diffusion models in few-shot segmentation. In *Proceedings of the NeurIPS 2023 Workshop on Diffusion Models*, 2023. URL <https://neurips.cc/virtual/2023/74849>. Poster.
- Luo, G., Dunlap, L., Park, D. H., Holynski, A., and Darrell, T. Diffusion hyperfeatures: Searching through time and space for semantic correspondence. *Advances in Neural Information Processing Systems*, 36:47500–47510, 2023.
- Ma, N., Goldstein, M., Albergo, M. S., Boffi, N. M., Vanden-Eijnden, E., and Xie, S. Sit: Exploring flow and diffusion-based generative models with scalable interpolant transformers. In *ECCV*, pp. 23–40, 2024.
- Misra, I. and Maaten, L. v. d. Self-supervised learning of pretext-invariant representations. In *Proceedings of the IEEE/CVF Conference on Computer Vision and Pattern Recognition*, pp. 6707–6717, 2020.
- Mizrahi, D., Bachmann, R., Kar, O., Yeo, T., Gao, M., Dehghan, A., and Zamir, A. 4m: Massively multimodal masked modeling. *Advances in Neural Information Processing Systems*, 36:58363–58408, 2023.
- Mukhopadhyay, S., Gwilliam, M., Agarwal, V., Padmanabhan, N., Swaminathan, A., Hegde, S., Zhou, T., and Shrivastava, A. Diffusion models beat gans on image classification, 2023.
- Nash, C., Menick, J., Dieleman, S., and Battaglia, P. W. Generating images with sparse representations. *arXiv preprint arXiv:2103.03841*, 2021.
- Nichol, A. Q. and Dhariwal, P. Improved denoising diffusion probabilistic models. In *ICML*, volume 139, pp. 8162–8171, 18–24 Jul 2021.
- Noroozi, M. and Favaro, P. Unsupervised learning of visual representations by solving jigsaw puzzles. In Leibe, B., Matas, J., Sebe, N., and Welling, M. (eds.), *ECCV*, pp. 69–84, 2016.
- Oquab, M., Darcet, T., Moutakanni, T., Vo, H. V., Szafraniec, M., Khalidov, V., Fernandez, P., HAZIZA, D., Massa, F., El-Nouby, A., Assran, M., Ballas, N., Galuba, W., Howes, R., Huang, P.-Y., Li, S.-W., Misra, I., Rabbat, M., Sharma, V., Synnaeve, G., Xu, H., Jegou, H., Mairal, J., Labatut, P., Joulin, A., and Bojanowski, P. DINOv2: Learning robust visual features without supervision. *Transactions on Machine Learning Research*, 2024. URL <https://openreview.net/forum?id=a68SUt6zFt>.
- Peebles, W. and Xie, S. Scalable diffusion models with transformers. In *Proceedings of the IEEE/CVF International Conference on Computer Vision*, pp. 4195–4205, 2023.

- Radford, A., Kim, J. W., Hallacy, C., Ramesh, A., Goh, G., Agarwal, S., Sastry, G., Askell, A., Mishkin, P., Clark, J., et al. Learning transferable visual models from natural language supervision. In *ICML*, 2021a.
- Radford, A., Kim, J. W., Hallacy, C., Ramesh, A., Goh, G., Agarwal, S., Sastry, G., Askell, A., Mishkin, P., Clark, J., et al. Learning transferable visual models from natural language supervision. In *International conference on machine learning*, pp. 8748–8763. PmlR, 2021b.
- Rombach, R., Blattmann, A., Lorenz, D., Esser, P., and Ommer, B. High-resolution image synthesis with latent diffusion models. In *CVPR*, pp. 10684–10695, 2022.
- Ronneberger, O., Fischer, P., and Brox, T. U-net: Convolutional networks for biomedical image segmentation. In *Medical image computing and computer-assisted intervention—MICCAI 2015: 18th international conference, Munich, Germany, October 5-9, 2015, proceedings, part III 18*, pp. 234–241. Springer, 2015.
- Salimans, T., Goodfellow, I., Zaremba, W., Cheung, V., Radford, A., and Chen, X. Improved techniques for training gans. *Advances in neural information processing systems*, 29, 2016.
- Tang, Z., Yang, Z., Zhu, C., Zeng, M., and Bansal, M. Any-to-any generation via composable diffusion. *Advances in Neural Information Processing Systems*, 36:16083–16099, 2023.
- Tian, K., Jiang, Y., Yuan, Z., Peng, B., and Wang, L. Visual autoregressive modeling: Scalable image generation via next-scale prediction. *arXiv preprint arXiv:2404.02905*, 2024.
- Tschannen, M., Gritsenko, A., Wang, X., Naeem, M. F., Alabdulmohsin, I., Parthasarathy, N., Evans, T., Beyer, L., Xia, Y., Mustafa, B., Hénaff, O., Harmsen, J., Steiner, A., and Zhai, X. Siglip 2: Multilingual vision-language encoders with improved semantic understanding, localization, and dense features. *arXiv preprint arXiv:2502.14786*, 2025.
- Tumanyan, N., Geyer, M., Bagon, S., and Dekel, T. Plug-and-play diffusion features for text-driven image-to-image translation. In *Proceedings of the IEEE/CVF Conference on Computer Vision and Pattern Recognition*, pp. 1921–1930, 2023.
- Van den Oord, A., Li, Y., and Vinyals, O. Representation learning with contrastive predictive coding. *arXiv e-prints*, pp. arXiv–1807, 2018.
- Vincent, P. A connection between score matching and denoising autoencoders. *Neural Computation*, 23(7):1661–1674, 2011. doi: 10.1162/NECO\_a\_00142.
- Xiang, W., Yang, H., Huang, D., and Wang, Y. Denoising diffusion autoencoders are unified self-supervised learners. In *Proceedings of the IEEE/CVF International Conference on Computer Vision*, pp. 15802–15812, 2023.
- Xie, Z., Zhang, Z., Cao, Y., Lin, Y., Bao, J., Yao, Z., Dai, Q., and Hu, H. Simmim: A simple framework for masked image modeling. In *Proceedings of the IEEE/CVF Conference on Computer Vision and Pattern Recognition (CVPR)*, pp. 9653–9663, 2022.
- Yang, X. and Wang, X. Diffusion model as representation learner. In *Proceedings of the IEEE/CVF International Conference on Computer Vision*, pp. 18938–18949, 2023.
- Yao, J., Wang, C., Liu, W., and Wang, X. Fasterdit: Towards faster diffusion transformers training without architecture modification. In *NeurIPS*, 2024.
- Yu, L., Lezama, J., Gundavarapu, N. B., Versari, L., Sohn, K., Minnen, D., Cheng, Y., Gupta, A., Gu, X., Hauptmann, A. G., Gong, B., Yang, M.-H., Essa, I., Ross, D. A., and Jiang, L. Language model beats diffusion - tokenizer is key to visual generation. In *The Twelfth International Conference on Learning Representations*, 2024.
- Yu, S., Kwak, S., Jang, H., Jeong, J., Huang, J., Shin, J., and Xie, S. Representation alignment for generation: Training diffusion transformers is easier than you think. In *ICLR*, 2025.
- Zhai, X., Mustafa, B., Kolesnikov, A., and Beyer, L. Sigmoid Loss for Language Image Pre-Training . In *ICCV*, pp. 11941–11952, 2023.

- Zhang, J., Herrmann, C., Hur, J., Polania Cabrera, L., Jampani, V., Sun, D., and Yang, M.-H. A tale of two features: Stable diffusion complements dino for zero-shot semantic correspondence. *Advances in Neural Information Processing Systems*, 36:45533–45547, 2023.
- Zhang, Q., Zhai, S., Bautista, M. A., Miao, K., Toshev, A., Susskind, J., and Gu, J. World-consistent video diffusion with explicit 3d modeling. *arXiv preprint arXiv:2412.01821*, 2024.
- Zhao, W., Rao, Y., Liu, Z., Liu, B., Zhou, J., and Lu, J. Unleashing text-to-image diffusion models for visual perception. In *Proceedings of the IEEE/CVF International Conference on Computer Vision*, pp. 5729–5739, 2023.
- Zheng, H., Nie, W., Vahdat, A., and Anandkumar, A. Fast training of diffusion models with masked transformers. *arXiv preprint arXiv:2306.09305*, 2023.
- Zhou, J., Wei, C., Wang, H., Shen, W., Xie, C., Yuille, A., and Kong, T. ibot: Image bert pre-training with online tokenizer. *International Conference on Learning Representations (ICLR)*, 2022.
- Zhu, R., Pan, Y., Li, Y., Yao, T., Sun, Z., Mei, T., and Chen, C. W. Sd-dit: Unleashing the power of self-supervised discrimination in diffusion transformer. In *CVPR*, pp. 8435–8445, 2024.

# Appendix

## Contents

<b>A ReDi with Stochastic Interpolant Models (SiT)</b>	<b>15</b>
A.1 Stochastic Interpolant Models (SiT)	15
A.2 Joint Image-Representation Generation with SiT	15
<b>B Additional Implementation Details</b>	<b>16</b>
B.1 Architecture details	16
B.2 Optimization details	16
B.3 Further implementation details	16
<b>C Detailed Benchmarks</b>	<b>16</b>
<b>D Baseline Generative Models</b>	<b>17</b>
<b>E Limitations &amp; Future Work</b>	<b>18</b>
<b>F Broader Impact</b>	<b>18</b>
<b>G Additional Qualitative Results</b>	<b>19</b>

## A ReDi with Stochastic Interpolant Models (SiT)

In the main paper, we introduced ReDi within the DDPM framework, as employed by DiT models. In this section, we begin with a brief overview of Stochastic Interpolant Models Ma et al. (2024) and then describe how ReDi can be applied in this setting.

### A.1 Stochastic Interpolant Models (SiT)

Following flow-based models Lipman et al. (2023), stochastic interpolants involve a continuous time-dependent process transforming a data distribution  $\mathbf{x}_0 \sim p(\mathbf{x})$  into Gaussian noise  $\epsilon \sim \mathcal{N}(\mathbf{0}, \mathbf{I})$ :

$$\mathbf{x}_t = \alpha_t \mathbf{x}_0 + \sigma_t \epsilon, \quad \alpha_0 = \sigma_1 = 1, \quad \alpha_1 = \sigma_0 = 0, \quad (14)$$

where  $\alpha_t$  and  $\sigma_t$  are increasing and decreasing functions of  $t$  respectively.

Given this process, the marginal probability distribution  $p_t(\mathbf{x})$  of  $\mathbf{x}_t$  in (14) coincides with the distribution of the probability flow ordinary differential equation with a velocity field:

$$\dot{\mathbf{x}}_t = \mathbf{v}(\mathbf{x}_t, t). \quad (15)$$

The velocity field can be approximated by a neural network  $\mathbf{v}_\theta(x_t, t)$  by minimizing the following training objective:

$$\mathcal{L}_{\text{velocity}}(\theta) := \mathbb{E}_{\mathbf{x}_0, \epsilon, t} \left\| \mathbf{v}_\theta(\mathbf{x}_t, t) - \dot{\alpha}_t \mathbf{x}_0 - \dot{\sigma}_t \epsilon \right\|^2. \quad (16)$$

### A.2 Joint Image-Representation Generation with SiT

During training, given a VAE latent image  $\mathbf{x}_0$  and a visual representation  $\mathbf{z}_0$ , we define a joint interpolation process:

$$\mathbf{x}_t = \alpha_t \mathbf{x}_0 + \sigma_t \epsilon_x, \quad \mathbf{z}_t = \alpha_t \mathbf{z}_0 + \sigma_t \epsilon_z, \quad (17)$$

The model  $\mathbf{v}_\theta(\mathbf{x}_t, \mathbf{z}_t, t)$  takes as input  $\mathbf{x}_t$  and  $\mathbf{z}_t$ , along with timestep  $t$ , and jointly predicts the velocity for both inputs. Specifically, it produces two separate predictions:  $\mathbf{v}_\theta^x(\mathbf{x}_t, \mathbf{z}_t, t)$  for the image latent velocity  $\mathbf{v}_x$ , and  $\mathbf{v}_\theta^z(\mathbf{x}_t, \mathbf{z}_t, t)$  for the visual representation velocity  $\mathbf{v}_z$ . The training objective combines both predictions:

$$\mathcal{L}_{joint} = \mathbb{E}_{\mathbf{x}_0, \mathbf{z}_0, t} \left[ \|\mathbf{v}_\theta^x(\mathbf{x}_t, \mathbf{z}_t, t) - \dot{\alpha}_t \mathbf{x}_0 - \dot{\sigma}_t \boldsymbol{\epsilon}_x\|^2 + \lambda_z \|\mathbf{v}_\theta^z(\mathbf{x}_t, \mathbf{z}_t, t) - \dot{\alpha}_t \mathbf{z}_0 - \dot{\sigma}_t \boldsymbol{\epsilon}_z\|^2 \right], \quad (18)$$

where  $\lambda_z$  balances the velocity loss for  $\mathbf{z}_t$ . By default, we use  $\lambda_z = 1$ ,  $\alpha_t = t$  and  $\sigma_t = 1 - t$  in our experiments.

## B Additional Implementation Details

### B.1 Architecture details

We present in Table 7 the configurations of the different-sized DiT and SiT models used in our experiments.

Table 7: **Model configuration details.** The configurations are the same for both DiT and SiT models.

MODEL SIZE	B/2	L/2	XL/2
Input Size	$32 \times 32 \times 4$	$32 \times 32 \times 4$	$32 \times 32 \times 4$
Patch Size	2	2	2
# Layers	12	24	28
# Heads	12	16	16
Hidden Dim.	768	1024	1152

### B.2 Optimization details

We present in Table 8 the optimization hyperparameters used for all experiments presented in the paper.

Table 8: **Optimization details.** The optimization hyperparameters for both DiT and SiT models.

Batch Size	256
Optimizer	AdamW
LR	$10^{-4}$
$(\beta_1, \beta_2)$	(0.9, 0.999)

**Computational Resources.** For both training and sampling we use 8 NVIDIA A100 40GB GPUs. Throughput, as presented in Table 6 is measured on a single NVIDIA A100 40GB GPU with a batch size of 64 as the number of images generated per second using 250 sampling steps.

### B.3 Further implementation details

**ReDi with REPA experiment.** To apply the Representation Alignment objective (REPA) on top of ReDi we follow the implementation of (Yu et al., 2025) and employ a projection layer in the 8th transformer layer. The projection is a three-layer MLP with SiLU activations (Elfwing et al., 2018). The weight on alignment loss is  $\lambda_{\text{REPA}} = 0.5$ .

## C Detailed Benchmarks

We provide a detailed evaluation of the main experiments presented in the main paper, including additional metrics and training iterations. Specifically, Table 9 details the performance of the SiT-XL/2 w/ ReDi models. Further Table 10 presents results for the ReDi with REPA (SiT-XL/2). For all models, we use the evaluation metrics reported in the original publications.

MODEL	#ITERS.	FID↓	sFID↓	IS↑	PREC.↑	REC.↑
SiT-XL/2 Peebles & Xie (2023)	7M	8.3	6.3	131.7	0.68	0.67
w/ ReDi	50K	56.1	18.9	23.8	0.44	0.47
w/ ReDi	100K	23.1	5.9	61.5	0.64	0.57
w/ ReDi	200K	12.6	5.7	97.3	0.69	0.61
w/ ReDi	300K	9.7	5.3	117.3	0.71	0.62
w/ ReDi	400K	7.5	5.1	129.5	0.72	0.62
w/ ReDi	4M	3.3	4.8	188.9	0.74	0.68

Table 9: **Detailed evaluation** for SiT-XL/2 w/ ReDi. All results are reported without classifier-free guidance.

MODEL	#ITERS.	FID↓	sFID↓	IS↑	PREC.↑	REC.↑
SiT-REPA-XL/2 Yu et al. (2025)	400K	7.9	5.1	122.6	0.70	0.65
SiT-REPA-XL/2	4M	5.9	5.7	157.8	0.70	0.69
w/ ReDi	50K	44.8	18.7	32.8	0.50	0.49
w/ ReDi	100K	15.2	5.6	85.3	0.68	0.59
w/ ReDi	200K	8.3	5.2	122.3	0.71	0.61
w/ ReDi	300K	6.3	5.1	140.6	0.73	0.62
w/ ReDi	400K	5.3	4.9	149.8	0.74	0.63
w/ ReDi	1M	3.5	4.64	177.9	0.75	0.69

Table 10: **Detailed evaluation** for ReDi with REPA. All results are reported without classifier-free guidance.

## D Baseline Generative Models

We provide here a brief description of the baseline approaches presented in the main paper. Specifically, we consider (a) *Autoregressive Models*, (b) *Latent Diffusion Models*, and (c) REPA (Yu et al., 2025) that also *leverages visual representations* to enhance generative performance.

### (a) Autoregressive Models

- VAR (Tian et al., 2024) proposes a scalable generative framework that autoregressively predicts higher-resolution image details from lower-resolution contexts across multiple scales.
- MagViTv2 (Yu et al., 2024) introduces a lookup-free quantization method enabling a large vocabulary that is able to improve the generation quality of autoregressive models.
- MAR (Li et al., 2024) proposes an autoregressive image generation framework that eliminates the need for vector quantization

### (b) Latent Diffusion Models

- LDM (Rombach et al., 2022) proposes latent diffusion models, modeling the image distribution in a compressed latent space produced by a KL- or VQ-regularized autoencoder.
- U-ViT-H/2 Bao et al. (2023) proposes a ViT-based (Dosovitskiy et al., 2021) latent diffusion model that incorporates skip connections.
- DiT Peebles & Xie (2023) proposes a pure transformer backbone for training diffusion models and incorporates AdaIN-zero modules.
- MaskDiT (Zheng et al., 2023) trains diffusion transformers with an auxiliary mask reconstruction task
- MDT Gao et al. (2023) introduce an effective mask latent modeling scheme, and design an asymmetric masking diffusion transformer.

- SD-DiT (Zhu et al., 2024) extends the MaskDiT architecture by incorporating a discrimination objective using a momentum encoder.
- SiT (Ma et al., 2024) improves diffusion transformer training by moving from discrete diffusion to continuous flow-based modeling.
- FasterDiT (Yao et al., 2024) incorporates supervision of the velocity direction into the denoising objective, significantly accelerating the training process.

### (c) Leveraging Visual Representations

- REPA (Yu et al., 2025) aligns the representations of diffusion transformer models to the representations of self-supervised models.

## E Limitations & Future Work

This section outlines some limitations of our current work and highlights promising directions for future research.

**Multiple visual representations.** In this work, we demonstrate the effectiveness of jointly modeling the visual representations from DINOv2 during the diffusion process. A promising direction for future research is to investigate whether integrating *multiple* visual representations, each capturing different semantic or structural properties, can further boost generative performance.

**Different dimensionality reduction approaches.** We have shown that projecting visual representations into a lower-dimensional space with PCA effectively compresses visual features while retaining sufficient information. An interesting direction for future work is to explore more sophisticated compression techniques, such as training an autoencoder, to better capture and retain the expressivity of these features.

## F Broader Impact

Generative models carry a substantial risk of misuse. Their application can lead to various negative societal impacts, most notably the spread of disinformation. Enhancements in generative performance, as achieved by our method, may further increase the realism of generated content, potentially making disinformation even more convincing.

## G Additional Qualitative Results

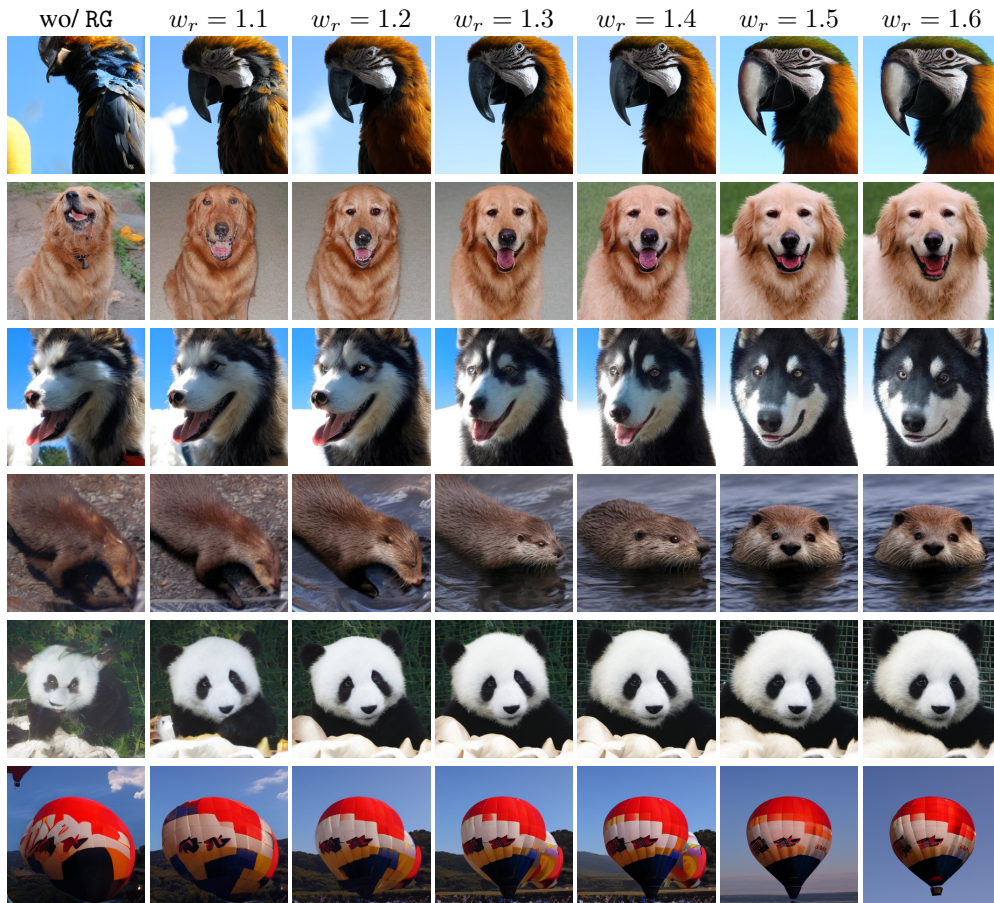


Figure 8: **The effect of Representation Guidance.** Samples from our DiT-XL/2 w/ ReDi model trained on ImageNet  $256 \times 256$  for 400k steps with different Representation Guidance weights  $w_r$ .



Figure 9: **Uncurated generation results** of SiT-XL/2 w/ ReDi. We use Classifier-Free Guidance with  $w = 4.0$ . Class label = 88.



Figure 10: **Uncurated generation results** of SiT-XL/2 w/ ReDi. We use Classifier-Free Guidance with  $w = 4.0$ . Class label = 89.



Figure 11: **Uncurated generation results** of SiT-XL/2 w/ ReDi. We use Classifier-Free Guidance with  $w = 4.0$ . Class label = 207.

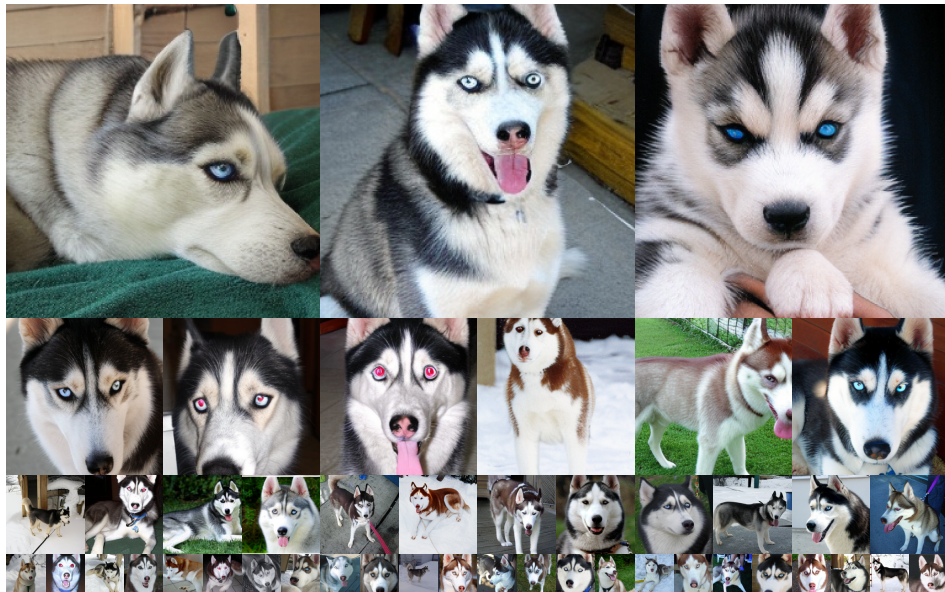


Figure 12: **Uncurated generation results** of SiT-XL/2 w/ ReDi. We use Classifier-Free Guidance with  $w = 4.0$ . Class label = 250.



Figure 13: **Uncurated generation results** of SiT-XL/2 w/ ReDi. We use Classifier-Free Guidance with  $w = 4.0$ . Class label = 417.



Figure 14: **Uncurated generation results** of SiT-XL/2 w/ ReDi. We use Classifier-Free Guidance with  $w = 4.0$ . Class label = 555.



Figure 15: **Uncurated generation results** of SiT-XL/2 w/ ReDi. We use Classifier-Free Guidance with  $w = 4.0$ . Class label = 928.



Figure 16: **Uncurated generation results** of SiT-XL/2 w/ ReDi. We use Classifier-Free Guidance with  $w = 4.0$ . Class label = 933.